The Impact of System Distortions and Noise on HV Backscatter and Its Relevance to Above-Ground Biomass Estimation from Spaceborne P-Band SAR Data

Zhirong Men, *Member, IEEE*, Shaun Quegan, Guido Riembauer, and Jie Chen, *Senior Member, IEEE*

***Abstract*—This article analyses the effects of system distortions (crosstalk and channel imbalance), Faraday rotation and system noise on estimates of the cross-polarized backscattering coefficient, σ^0_{hv}, by a spaceborne synthetic aperture radar. Modeling the unknown system errors and noise by a joint complex Gaussian distribution allows analytic first-order approximations to the mean and variance of the error in σ^0_{hv} to be derived that do not depend on the SAR operating frequency. Simulation shows these approximations to be very accurate, given the statistical model and the expected magnitudes of system errors and noise for the P-band instrument to be carried by the European Space Agency BIOMASS mission. Simulation further shows that the σ^0_{hv} errors are Gaussian distributed, so their exceedance probabilities can be calculated from just the analytic expressions for the mean and variance of the errors. Exceedance probabilities for above-ground biomass (AGB) can then be calculated under a power law relation between $\sigma^0_{\mathrm{hv}}\sigma_{\mathrm{hv}}$ and AGB that is consistent with P-band observations. This allows tradeoff curves between crosstalk and channel imbalance (shown to be segments of hyperbolas) to be calculated, along which the relative error in AGB is within a given percentage of its true value, from which limits on the permissible size of the errors can be determined if BIOMASS mission requirements are to be met.**

***Index Terms*—BIOMASS, biomass estimation error, P-band synthetic aperture radar (SAR), polarimetric measurement, system distortion.**

I. Introduction

EUROPEAN Space Agency (ESA)'s seventh earth explorer mission, BIOMASS, which is planned for launch in 2022, aims to improve the estimates of terrestrial carbon sources and sinks by quantifying the global distribution and changes of above-ground biomass (AGB) [1], [2]. The synthetic aperture radar (SAR) system operates at P-band, which gives higher sensitivity to AGB than shorter wavelengths and allows the signal to penetrate deep into or through the forest canopy. However, the signal is degraded by system distortions (channel imbalance and crosstalk), noise and Faraday rotation (FR). Channel imbalance describes the system-induced deviation of the amplitude ratio of the horizontally and vertically polarized channels from unity and their phase difference from zero. Crosstalk is an unwanted coupling between polarization signal paths. Both are treated separately for the transmit and receive channels [3]. In [4], a first-order analysis of how these effects combine to degrade measurements of the polarimetric backscattering coefficients in the presence of noise and FR was developed. These errors were then translated into an associated bias in AGB estimation under a power law relation between AGB and the cross-polarised backscattering coefficient σ^0_{hv}. This allowed identification of the maximum permissible amplitudes of channel imbalance and crosstalk in order to guarantee that the AGB estimation error did not exceed a given limit. The system performance requirements imposed on industry by ESA are based on these values.

However, the analysis in [4] identified worst case limits of channel imbalance and crosstalk by searching over uncorrelated uniform distributions for the amplitudes and phases of the distortion terms and FR angle, rather than a more realistic model of their statistical distributions. Also, only covariance matrices derived from airborne P-band campaign data over boreal forests (as embodied in the BIOMASS End-to-End Mission Performance Simulator [5]), were used to simulate polarimetric data, but none from tropical campaigns. This article addresses both these limitations.

After describing the system model in Section II, we show that the analysis in [4] can be extended to provide first-order analytic expressions for the mean and variance of the error in σ^0_{hv} under a joint Gaussian statistical model of the system errors, FR and noise (see Section III). A simulation strategy for estimating the σ^0_{hv} errors, given this statistical model, is described in Section IV. Simulation results in Section V confirm that the first-order expressions very accurately approximate the true mean and variance of the σ^0_{hv} errors over the range of crosstalk and channel imbalance errors expected for the BIOMASS system. Simulation also indicates that the σ^0_{hv} error distribution is

Manuscript received September 16, 2020; revised December 10, 2020 and January 30, 2021; accepted March 24, 2021. Date of publication April 6, 2021; date of current version April 22, 2021. This work was supported in part supported by ESA under Contract 4000116784/15/NL/CT. *(Corresponding author: Zhirong Men.)*

Zhirong Men and Jie Chen are with the School of Electronic and Information Engineering, Beihang University, Beijing 100191, China (e-mail: menzhirong@buaa.edu.cn; chenjie@buaa.edu.cn).

Shaun Quegan is with the School of Mathematics and Statistics, The University of Sheffield, S37RH Sheffield, U.K. (e-mail: s.quegan@sheffield.ac.uk).

Guido Riembauer is with the European Space Research and Technology Centre ESTEC, Noordwijk 2201AZ, The Netherlands (e-mail: guido.riembauer@gmail.com).

Digital Object Identifier 10.1109/JSTARS.2021.3071182

very close to Gaussian, so is completely characterized by its mean and variance. The analytic first-order expressions for the mean and variance of the $\sigma^0_{\rm hv}$ errors are then used to develop tradeoff curves between crosstalk and channel imbalance for given exceedance levels of the $\sigma^0_{\rm hv}$ error. These are applicable to any polarimetric SAR system, whatever its frequency. However, in order to relate this analysis to AGB estimates from the P-band BIOMASS SAR, we assume a power law relation between AGB and $\sigma^0_{\rm hv}$; this allows the tradeoff curves to be expressed in terms of relative error in AGB. The numerical calculations use values of polarimetric covariance and power law exponent derived from boreal and tropical airborne P-band campaign data. The relation of these findings to the conclusions in [4] about required BIOMASS system performance is discussed in Section VI, together with limitations of our analysis given the current status of AGB estimation algorithms for BIOMASS. Our conclusion is in Section VII.

II. System Model

The relationship between system errors, FR, noise and the scattering matrix *S* is given in [3] and regrouped in [4] as

$$\begin{bmatrix} M_{\rm hh} \\ M_{\rm hv} \\ M_{\rm vh} \\ M_{\rm vv} \end{bmatrix} = \begin{bmatrix} 1 & \delta_2 & \delta_4 & \delta_2\delta_4 \\ \delta_1 & f_1 & \delta_1\delta_4 & f_1\delta_4 \\ \delta_3 & \delta_2\delta_2 & f_2 & f_2\delta_2 \\ \delta_1\delta_3 & f_1\delta_3 & f_2\delta_1 & f_1 f_2 \end{bmatrix} \times \begin{bmatrix} c^2 & cs & -cs & -s^2 \\ -cs & c^2 & s^2 & -cs \\ cs & s^2 & c^2 & cs \\ -s^2 & cs & -cs & c^2 \end{bmatrix} \begin{bmatrix} S_{\rm hh} \\ S_{\rm hv} \\ S_{\rm vh} \\ S_{\rm vv} \end{bmatrix} + \begin{bmatrix} N_{\rm hh} \\ N_{\rm hv} \\ N_{\rm vh} \\ N_{\rm vv} \end{bmatrix} \quad (1)$$

where M_{pq}, S_{pq}, and N_{pq}, with *p* and *q* being either *h* or *v*, are the components of the measured scattering matrix, true scattering matrix and additive noise, respectively; f_i, $i = 1 - 2$, are channel imbalance terms; δ_i, $i = 1 - 4$, are crosstalk terms; and $c = \cos\Omega$, $s = \sin\Omega$, where Ω is the FR angle. Note that we have omitted the scalar factor, $Ae^{j\phi}$, describing the radar gain and phase delay [3] as the analysis focuses on polarimetric rather than absolute calibration. Since f_1 and f_2 are very close to 1, the channel imbalance terms can be rewritten as $f_i = 1 + \varepsilon_i$, $i = 1$, 2, where the ε_i are complex and of small amplitude. For natural targets we expect $S_{\rm hv} = S_{\rm vh}$, but the effects of FR, system errors and noise break this equality in the measured signal.

The maximum likelihood estimate of the S_{pq} given the measured values $M_{\boldsymbol{pq}}$ is derived in [4]. Of particular importance in biomass estimation is the estimated cross-polarized scattering matrix [6], given by

$$\hat{S}_{\rm hv} = \frac{M_{\rm hv} + M_{\rm vh}}{2} \quad (2)$$

which does not depend on an estimate of the FR angle Ω.

Equation (1) is appropriate for a point target but we are often more interested in distributed targets, which are characterized by a covariance matrix *C*, where

$$C\,(i,\ j) = \langle S_i S_j^* \rangle$$

with $\langle\cdot\rangle$ denoting expectation and $*$ complex conjugate. The diagonal terms in *C* are denoted as $\sigma_{\rm hh}$, $\sigma_{\rm hv}$, $\sigma_{\rm vh}$, and $\sigma_{\rm vv}$, where $\sigma_{pq} = \langle |S_{pq}|^2 \rangle$. For natural targets we expect $\sigma_{\rm hv} = \sigma_{\rm vh}$. Note that we here use the notation σ_{hv} rather than $\sigma^0_{\rm hv}$, and similarly for the HH and VV channels, since the analysis does not depend on having radiometrically calibrated data. However, the simulations reported in Sections IV and V do require the use of reported values of the backscattering coefficients (see Table I) because they involve comparison with noise equivalent sigma zero (NESZ).

TABLE I
COVARIANCE MATRIX VALUES FOR FOREST OF DIFFERENT BIOMASS VALUES

Biome	AGB (t /ha)	σ^0_{hh} (m^2/m^2)	σ^0_{hv} (m^2/m^2)	σ^0_{vv} (m^2/m^2)	R	θ (degs.)
Boreal	50	0.213	0.0404	0.250	0.086	-54.6
	200	0.649	0.0726	0.274	0.150	-96.8
	350	1.018	0.0919	0.281	0.172	-139.1
Tropical	338	0.127	0.0482	0.145	0.022	-21.0
	341	0.182	0.086	0.186	0.042	-15.9

III. Mean and Variance of the Error in the Cross-Polarized Backscattering Coefficient

From (1), given the scattering vector $\boldsymbol{S}$, the values of the system errors and Ω, and a realization of the noise terms, we can calculate the measured scattering vector $\boldsymbol{M}$ and hence the errors in the components of $\boldsymbol{S}$. More generally, given the covariance matrix of a distributed target and the joint distribution of the errors, FR and noise, we can use simulation to derive the moments and joint distribution of these errors and the errors in the covariance terms. However, simulation may yield little insight into the most important controls on the errors, so in this section we derive analytic first-order approximations to the mean and variance of the error in $\sigma_{\rm hv}$ under the following assumptions about the joint distribution of system errors, noise and FR. These are in part guided by advice from Airbus U.K., who lead the consortium building the BIOMASS satellite.

1) δ_i and $\delta_4\varepsilon_i$ obey a joint zero-mean circular complex Gaussian distribution;
2) Only correlations are between the pairs of variables δ_1 and δ_3, δ_2 and δ_4, and ε_1 and ε_2;
3) N_{pq} are identically distributed independent complex zero-mean circular complex variables;
4) Ω has mean and variance that depend on location and time.

The Gaussian assumption is used only to simplify the variance calculation, since the expression derived for the mean relies solely on the system errors being zero-mean.

Note that this joint distribution describes different types of uncertainty. The system errors are expected to be fairly stable and have magnitudes within bounds that depend on the precision of the system engineering, but with unknown phase; the distribution describes our lack of knowledge about their exact values. FR is a geophysical phenomenon with large temporal and spatial variability but known climatology, so its general

statistical properties can be quantified. Noise is a random process characterized by the NESZ.

The error in $\sigma_{\rm hv}$ is given by $e = \hat{\sigma}_{\rm hv} - \sigma_{\rm hv}$, where $\hat{\sigma}_{\rm hv} = \langle|\hat{S}_{\rm hv}|^2\rangle$ and $\hat{S}_{\rm hv}$ is given by (2). Under the assumption of distributed targets with reflection symmetry, a first-order expression for this error was derived in [4] (13) for given values of the system errors and FR

$$\begin{aligned} e = {} & \sigma_{\rm hv}\left(2\,{\rm Re}(\Sigma_\varepsilon) + |\Sigma_\varepsilon|^2\right) \\ & + \sigma_{\rm hh}\left|c^2\Sigma_{13} - s^2\Sigma_{24}\right|^2 + \sigma_{\rm vv}\left|c^2\Sigma_{24} - s^2\Sigma_{13}\right|^2 \\ & + c^2s^2\left(\sigma_{\rm hh} + \sigma_{vv} + 2R\cos\theta\right)|Y_{21}|^2 \\ & + 2\,{\rm Re}\left\{\left(c^2\Sigma_{13} - s^2\Sigma_{24}\right)\left(c^2\Sigma^*_{24} - s^2\Sigma^*_{13}\right){\rm Re}^{j\theta}\right\} \\ & + 2cs\,{\rm Re}\left\{Y^*_{21}\left[\left(c^2\Sigma_{13} - s^2\Sigma_{24}\right)\left(\sigma_{\rm hh} + Re^{j\theta}\right)\right.\right. \\ & \left.\left. + \left(c^2\Sigma_{24} - s^2\Sigma_{13}\right)\left(\sigma_{\rm vv} + {\rm Re}^{-j\theta}\right)\right\} + \sigma_n/2 \end{aligned} \tag{3}$$

where $\Sigma_{13} = (\delta_1 + \delta_3)/2$, $\Sigma_{24} = (\delta_2 + \delta_4)/2$, $\Sigma_\varepsilon = (\varepsilon_1 + \varepsilon_2)/2$, $\Upsilon_{21} = (\varepsilon_2 - \varepsilon_1)/2$ and $\langle S_{\rm hh}S^*_{\rm vv}\rangle = {\rm Re}^{j\theta}$.

Setting

$$\begin{aligned} X &= c^2\,\Sigma_{13} - s^2\Sigma_{24} \\ Y &= c^2\,\Sigma_{24} - s^2\Sigma_{13} \\ A &= \Sigma_\varepsilon \\ B &= csY_{21} \\ P &= \sigma_{\rm hh} + \sigma_{\rm vv} + 2R\cos\theta \end{aligned} \tag{4}$$

(3) can be written:

$$\begin{aligned} e = {} & \sigma_{\rm hv}\left(2\,{\rm Re}\,(A) + |{\rm A}|^2\right) + P|B|^2 \\ & + 2{\rm Re}\left\{B^*\left[X\left(\sigma_{\rm hh} + Re^{j\theta}\right) + Y\left(\sigma_{\rm vv} + Re^{-j\theta}\right)\right]\right\} \\ & + \sigma_{\rm hh}|X|^2 + \sigma_{\rm vv}|Y|^2 + 2\,{\rm Re}\left\{{\rm Re}^{j\theta}XY^*\right\} + \sigma_n/2. \end{aligned} \tag{5}$$

A. Moments of X, Y, A, and B

From the statistical assumptions given above, the variances and covariance of *X* and *Y* are

$$V_X = \langle c^4\rangle V_{13} + \langle s^4\rangle V_{24} \tag{6a}$$

$$V_Y = \langle s^4\rangle V_{13} + \langle c^4\rangle V_{24} \tag{6b}$$

$$C_{XY} = \langle XY^*\rangle = C_{XY} = -\langle c^2s^2\rangle\left(V_{13} + V_{24}\right) \tag{6c}$$

where V_X, V_Y, V_{13} and V_{24} are the variances of *X, Y,* Σ_{13} and Σ_{24} respectively. Note that C_{XY} is real.

These quantities are related to the covariance statistics of the crosstalk distribution by

$$V_{13} = \langle|\Sigma_{13}|^2\rangle = \frac{1}{4}\left(V_1 + V_3 + 2{\rm Re}\left(C_{13}\right)\right) \tag{7a}$$

$$V_{24} = \langle|\Sigma_{24}|^2\rangle = \frac{1}{4}\left(V_2 + V_4 + 2{\rm Re}\left(C_{24}\right)\right) \tag{7b}$$

where V_i is the variance of δ_i, $C_{13} = \langle\delta_1\delta^*_3\rangle$ and $C_{24} = \langle\delta_2\delta^*_4\rangle$.

The corresponding results for *A* A and *B* B are

$$V_A = \frac{1}{4}\left(V_{\varepsilon 1} + V_{\varepsilon 2} + 2{\rm Re}\left(C_{\varepsilon 12}\right)\right) \tag{8a}$$

$$V_B = \frac{1}{4}\langle c^2s^2\rangle\left(V_{\varepsilon 1} + V_{\varepsilon 2} - 2{\rm Re}\left(C_{\varepsilon 12}\right)\right) \tag{8b}$$

$$C_{AB} = \langle AB^*\rangle = \frac{\langle cs\rangle}{4}\left(V_{\varepsilon 2} - V_{\varepsilon 1} + 2j\,{\rm Im}\left(C_{\varepsilon 12}\right)\right) \tag{8c}$$

where $V_{\varepsilon i}$ is the variance of ε_i and $C_{\varepsilon 12} = \langle\varepsilon_1\,\varepsilon^*_2\rangle$.

B. Moments of the Trigonometric Functions of Ω

The above expressions contain the following moments of trigonometric functions of Ω

$$\langle c^4\rangle = \left(3 + 4\langle\cos 2\Omega\rangle + \langle\cos 4\Omega\rangle\right)/8 \tag{9a}$$

$$\langle s^4\rangle = \left(3 - 4\langle\cos 2\Omega\rangle + \langle\cos 4\Omega\rangle\right)/8 \tag{9b}$$

$$\langle c^2s^2\rangle = \left(1 - \langle\cos 4\Omega\rangle\right)/8 \tag{9c}$$

$$\langle cs\rangle = \langle\sin 2\Omega\rangle/2. \tag{9d}$$

These can be easily calculated if Ω is Gaussian distributed with mean $\langle\Omega\rangle$ and standard deviation (SD) σ_Ω , in which case

$$\langle\cos p\Omega\rangle = \cos\left(p\langle\Omega\rangle\right)\exp\left(-\sigma^2_\Omega\,p^2/2\right) \tag{10}$$

This is only approximate because Ω is a circular variable, but is acceptable if σ_Ω is not too large and $\langle\Omega\rangle$ is not too close to π (taking Ω between $-\pi$ and π). Note that near the magnetic equator $\langle\Omega\rangle$ will be near zero and σ_Ω will be small, but both the magnitude of the mean and σ_Ω will increase as we move away from the equator.

C. Mean and Variance of the Error in $\sigma_{\rm hv}$

We can now assemble the expected value of (5) over the system error and FR angle distributions (for details see Appendix A):

$$\langle e\rangle = \sigma_{\rm hv}V_A + PV_B + \sigma_{\rm hh}V_X + \sigma_{\rm vv}V_Y + 2R\cos\theta C_{XY} + \frac{\sigma_n}{2} \tag{11}$$

where *P*, V_A, V_B, V_X, V_Y and C_{XY} are given by (4), (6) and (8).

Equation (11) relies only on the assumption that the complex system errors are zero-mean with the correlation properties discussed above, but makes no further assumptions about their distributions. With the extra assumption that they obey a circular Gaussian distribution, *X*, *Y*, *A,* and *B* will also be circular zero-mean Gaussian. The variance of the error in $\sigma_{\rm hv}$, i.e., $V_e = \langle(e - \langle e\rangle)^2\rangle$, is then given by the sum of three terms (details are given in Appendix A)

$$V_{e1} = \sigma^2_{\rm hv}\left(V^2_A + 2V_A\right) + P^2V^2_B + 2\sigma_{\rm hv}P|C_{AB}|^2 \tag{12a}$$

$$\begin{aligned} V_{e2} = {} & \sigma^2_{\rm hh}V^2_X + \sigma^2_{vv}V^2_Y + 2R^2\left\{V_XV_Y + C^2_{XY}\cos 2\theta\right\} \\ & + 2\sigma_{\rm hh}\sigma_{\rm vv}C^2_{XY} + 4R\cos\theta C_{XY}\left(\sigma_{\rm hh}V_X + \sigma_{\rm vv}V_Y\right) \end{aligned} \tag{12b}$$

$$V_{e3} = 2V_B\{V_X\sigma^2_{\rm hh} + V_Y\sigma^2_{\rm vv} + 2C_{XY}\sigma_{hh}\sigma_{vv}$$

$$+ 2R\cos\theta\left(V_X\sigma_{\rm hh} + V_Y\sigma_{\rm vv} + C_{XY}\left(\sigma_{\rm hh} + \sigma_{vv}\right)\right)$$
$$+ R^2\left(V_X + V_Y + 2C_{XY}\cos 2\theta\right)\}. \tag{12c}$$

The first comes purely from channel imbalance, the second from crosstalk, while the third is an interaction term.

The expressions in (11) and (12) can be simplified if we assume the crosstalk terms all have the same variance, i.e., $V_i = V_\delta$ for all i, and the complex correlation coefficients of δ_1 and δ_3, δ_2 and δ_4 are $\rho_{13} = \rho_{24} = C_{13}/V_\delta = C_{24}/V_\delta = \rho_\delta$. We write $\angle\rho_\delta = \theta_\delta$. Then we have

$$V_X = V_Y = \frac{V_\delta}{8}\left(1 + |\rho_\delta|\cos\theta_\delta\right)\left(3 + \langle\cos 4\Omega\rangle\right) \tag{13a}$$

$$C_{XY} = C_{YX} = -\frac{V_\delta}{8}\left(1 + |\rho_\delta|\cos\theta_\delta\right)\left(1 - \langle\cos 4\Omega\rangle\right). \tag{13b}$$

Similarly, with similar notation

$$V_A = \frac{V_\varepsilon}{2}\left(1 + |\rho_\varepsilon|\cos\theta_\varepsilon\right) \tag{14a}$$

$$V_B = \langle c^2 s^2\rangle\frac{V_\varepsilon}{2}\left(1 - |\rho_\varepsilon|\cos\theta_\varepsilon\right) \tag{14b}$$

$$C_{AB} = j\langle cs\rangle\frac{V_\varepsilon}{2}|\rho_\varepsilon|\sin\theta_\varepsilon. \tag{14c}$$

These expressions can be substituted into (11) and (12) to give the mean and variance of the error in σ_{hv} in terms of the variances and correlation coefficients of the δ_i and ε_i.

Note that the unknown phase of the system error correlation coefficients has significant effects. For example, (12b) has a maximum and minimum when $\theta_\delta = 0$ and π respectively, since these values of θ_δ maximise and minimize the expressions in (13a) and (13b). If the magnitude of the correlation coefficients is near 1, (12b) is nearly 0 when $\theta_\delta = \pi$. Similarly, the value of (12a) is maximised when $\theta_\varepsilon = 0$, in which case for ρ_ε near 1, $V_A \approx V_\varepsilon$ and V_B and C_{AB} are both nearly 0, and it is minimised when $\theta_\varepsilon = \pi$, in which case V_A and C_{AB} are both nearly 0 and $V_B \approx \langle c^2 s^2\rangle V_\varepsilon$.

D. Relation Between Error in $\boldsymbol{\sigma_{\rm hv}}$ and Error in AGB

The error in $\sigma_{\rm hv}$ can be related to the error in AGB, denoted as B, under a power law for AGB [6]

$$B = A\sigma_{\rm hv}^p. \tag{15}$$

An erroneous estimate of B B can be written as $\hat{B} = (1+q)B$ and the corresponding estimate of $\sigma_{\rm hv}$ is given by

$$A\hat{\sigma}_{\rm hv}^p = (1+q)\,A\sigma_{\rm hv}^p.$$

The relative error in B is then

$$\frac{\hat{B} - B}{B} = q = \frac{\hat{\sigma}_{\rm hv}^p - \sigma_{\rm hv}^p}{\sigma_{\rm hv}^p}.$$

Hence the corresponding relative error in $\sigma_{\rm hv}$ is

$$\frac{\hat{\sigma}_{\rm hv} - \sigma_{\rm hv}}{\sigma_{\rm hv}} = (1+q)^{1/p} - 1. \tag{16}$$

Typical values of p for boreal and tropical forests are 2.2 and 1.9, respectively [6]. The relative errors in σ_{hv} yielding a 20% overestimate in AGB are 0.0864 in the first case and 0.101 in the second, while for a 20% underestimate they are -0.0965 and -0.1108 respectively. This implies two things: requirements for system accuracy are more stringent in boreal forests than in tropical forests; and because the $\sigma_{\rm hv}$ errors have a symmetric distribution (see Section V-A), constraining the system errors to keep overestimates of AGB below a given relative level will automatically have the same effect for underestimates. The second point is reinforced by the fact that the error distribution has a positive mean (11).

IV. Numerical Simulations

The accuracy of the first-order approximations developed in Section III was tested by simulating the measurement process directly from (1) without making any approximations. Table I gives the covariance values used in the simulation for three boreal forest biomass values (50, 200, and 350 t/ha) [4] and two tropical biomass values (338 t/ha from TropiSAR [7] and 341 t/ha from AfriSAR [8]). The latter are both for dense forest because this was the focus of the tropical campaigns.

The simulation involves three steps:

1) *Scene Generation:* A homogeneous "scene" consisting of L independent samples of scattering vectors $S(k)$, $k \in [1, L]$, drawn from a zero-mean complex Gaussian distribution characterized by the covariance values in Table I, is generated using Choleski decomposition. The associated estimate of $\sigma_{\rm hv}^0$ is

$$\sigma_{\rm hv}^0 = \frac{1}{L}\sum_{k=1}^{L}|S_{\rm hv}(k)|^2. \tag{17}$$

The value of L is chosen to be large enough that this gives a very good approximation to the true value of $\sigma_{\rm hv}^0$, so we use the same notation for both.

2) *Generate M Joint Samples of System Errors and FR, and N Joint Samples of Noise: M* independent realizations of the combined system errors and FR are generated under the statistical model given in Section III. Each of these is applied to all the pixels in the simulated scene. An independent realization of the noise vector for a given NESZ is then added to each pixel. This corresponds to a single realization of the measured scene under the system model (1) in which all the pixels suffer the same system distortion and FR, but where each pixel is independently affected by noise. The effects of system noise can then be simulated by holding the system errors and FR fixed, and adding new noise realizations to each pixel, an operation carried out N times. This yields $M \times N$ simulations of the measured scene.
3) *Statistics of the Error in $\sigma_{\rm hv}^0$:* Given the ensemble of simulated scene measurements and the estimate (17) we can calculate the mean and variance of the error in $\sigma_{\rm hv}^0$ and compare them with the predictions in Section III. The

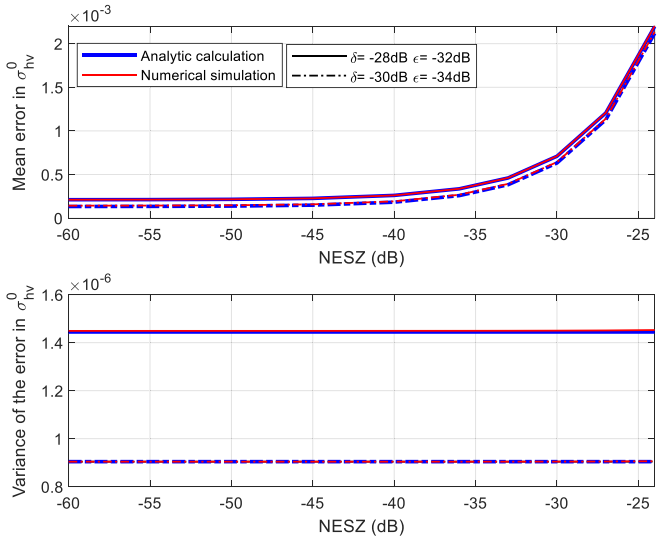

Fig. 1. Mean and variance of the error in $\sigma^0_{\rm hv}$ for a boreal biomass of 200 t/ha as NESZ varies under Gaussian distributed FR with mean $\pi/3$ and SD $\pi/36$, shown for two different levels of system distortions indicated by different line styles.

simulation also provides information on the distribution of errors in $\sigma^0_{\rm hv}$.

In the following simulations we fix $L = 100000$, $M = 10000$, and $N = 1$. The correlation coefficient of both the crosstalk and channel imbalance terms is fixed as $\rho = 0.9e^{j0}$ ($\angle\rho = 0$ is the most stringent situation, see Section III-C).

V. Results

A. Testing the Predictions of the $\boldsymbol{\sigma_{\rm hv}}$ Error Statistics

The bias and variance of the error in $\sigma_{\rm hv}$ calculated using both numerical simulation and (11) and (12) are shown in Fig. 1 for a boreal biomass of 200 t/ha (see Table I) under Gaussian distributed FR with mean $\pi/3$ and SD $\pi/36$, and two levels of system error, with mean zero and $V_\delta = -30$ dB, $V_\varepsilon = -34$ dB and $V_\delta = -28$ dB, $V_\varepsilon = -32$ dB (this 4 dB difference is based on the observation in [4] that the channel imbalance term needs to be smaller than crosstalk to yield similar errors in biomass). Note that the accuracy of the predictions using the analytic calculation does not depend on this 4 dB difference.

For NESZ < -35 dB the bias is almost entirely due to system errors, but as NESZ increases beyond this point the relative contribution of noise to the bias increases rapidly. When NESZ $= -27$ dB (the specification for the BIOMASS instrument) noise is a factor 2.1 and 1.7 greater than the system error for the lower curves and upper curves, respectively.

The theoretical and simulated bias are very similar (they can barely be distinguished in Fig. 1) so we can use (11), (13) and (14) to calculate the contribution to the bias by system errors as 1.43×10^{-4} (lower curves) and 2.11×10^{-4} (upper curves). The crosstalk contribution to the bias is an order of magnitude greater than that from channel imbalance (this is true for all five biomass values in Table I; see Appendix C). The lower panel in Fig. 1 shows that the variance is independent of the noise, as predicted by (12), and the simulated value of the variance is very close to the analytic value. Similar behavior is seen for all the cases given in Table I over a range of conditions on the FR angles.

Table II
Relative Error in the Bias and Variance of Estimated $\sigma^0_{\rm hv}$

Crosstalk (dB)	Channel imbalance (dB)	Biomass (t/ha)	Mean FR (degree)	Relative difference of the bias	Relative difference of the variance
-28	-32	200	60	0.22%	0.44%
-28	-32	338	0	0.40%	0.11%
-30	-34	50	30	1.32%	0.38%
-30	-34	200	60	1.04%	0.07%
-30	-34	350	90	0.84%	-0.65%
-30	-34	338	0	0.44%	0.41%
-30	-34	341	0	0.46%	0.25%
-28	-28	200	60	0.34%	0.34%
-30	-30	200	60	0.36%	0.26%
-32	-32	200	60	0.80%	0.84%

The relative differences in the bias and variance between the simulations and analytic expression are defined as

$$\frac{\text{Bias}_{\text{numerical}} - \text{Bias}_{\text{analytic}}}{\text{Bias}_{\text{analytic}}} \tag{18a}$$

$$\frac{V_{\text{numerical}} - V_{\text{analytic}}}{V_{\text{analytic}}}. \tag{18b}$$

Table II gives their values for calculations like those illustrated in Fig. 1 for all the AGB values in Table I when NESZ $= -27$dB and for several FR angles. The relative differences are all below 1.32% for bias and 0.84% for variance, and for the boreal data tend to decline as AGB increases. These results confirm that under the assumed statistical model the analytical approach provides very accurate estimates of both the bias and variance of the $\sigma^0_{\rm hv}$ errors given the target covariance, the variance-covariance properties of crosstalk and channel imbalance, the mean and variance of FR, and the NESZ. The last three entries in Table II also illustrate that the difference between crosstalk and the channel imbalance term is not a significant control on the accuracy.

In order to fully exploit this we need to know the $\sigma^0_{\rm hv}$ error distribution, but this can be measured from the simulations, as shown in Fig. 2 for an AGB of 200 t/ha with a range of noise levels when the levels of crosstalk and the channel imbalance terms are -30 and -34 dB, respectively. Gaussian distributions parameterized by the estimated mean and variance (superimposed in red) clearly provide very good approximations to the histograms. The increasing bias as NESZ increases is also clear.

B. Tradeoff Curves for Crosstalk and Channel Imbalance

Because the $\sigma^0_{\rm hv}$ error distribution is well approximated by a Gaussian distribution parameterized by the first-order estimates of the mean and variance of the error (see Section V-A), we can calculate exceedance probabilities using standard Gaussian tables. For example, the probability of error exceeds $\alpha = 5\%, 1\%,$ and 0.135% when the standardized error, $z_\alpha = (e - \langle e\rangle)/\sigma_e$, exceeds the values $z_\alpha = 1.65, 2.33,$ and 3.00, respectively (here, σ_e is the SD of the error). These values relate to overestimates;

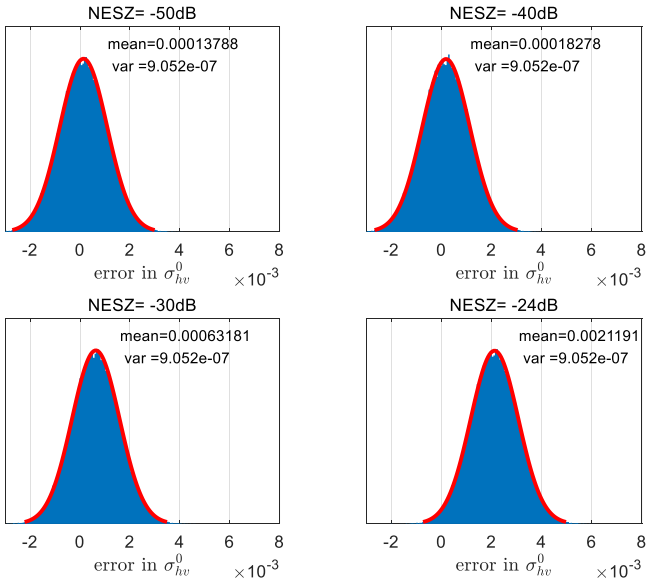

Fig. 2. Histograms of the error in $\sigma^0_{\rm hv}$ for an AGB of 200 t/ha and a range of values of NESZ when the crosstalk and the channel imbalance terms have values -30 and -34 dB, respectively, derived by simulation of (1). The red curve is a Gaussian distribution parameterized by the mean and variance estimated from the simulated errors.

the corresponding standardized errors for underestimates are -1.65, -2.33, and -3.00.

The combinations of the channel imbalance and crosstalk variances that keep the error in $\sigma^0_{\rm hv}$ below $f\sigma^0_{\rm hv}$, i.e., a given fraction f of $\sigma^0_{\rm hv}$, with probability α, are therefore given by solving

$$b\left(V_\delta,\ V_\varepsilon\right) + z_\alpha \sigma_e\left(V_\delta,\ V_\varepsilon\right) = f\sigma^0_{\rm hv} \tag{19}$$

where $b(V_\delta,\ V_\varepsilon) = \langle e \rangle$ is the mean error (bias) and z_α is the standardized error giving an exceedance probability α under a one-sided test. As explicitly indicated, both b and σ_e are functions of V_δ and V_ε. It is shown in Appendix B that the tradeoff curve (19) is a segment of a hyperbola.

Although the magnitude of the errors in the ε_i and δ_i can be quantified by their variances V_ε and V_δ, we instead characterize them by the probability that their amplitudes, $|\varepsilon_i|$ and $|\delta_i|$, are less than 3σ, where σ is the SD of the real and imaginary parts of the errors. This is because industry prefers to quantify system error uncertainty in terms of amplitude. Under the Gaussian assumption, the amplitudes obey Rayleigh distributions, so have cumulative density functions of the form

$$P_{|\delta|}\left(x\right) = p\left\{|\delta| < x\right\} = 1 - \exp\left(-x^2/\left(2\sigma^2\right)\right), \tag{20}$$

Hence, the probability that the amplitude error exceeds 3σ is 0.01111. The tradeoff curves displayed in the next section are labeled in terms of the associated dB value given by $10\log_{10}(3\sigma)^2 = 10\log_{10}(9V_\delta/2)$ (with similar expressions for the channel imbalance terms).

It should be noted that up to this point the results deal only with the HV backscattering coefficient, so are equally applicable to any spaceborne polarimetric SAR system, whatever its frequency. This includes the tradeoff (19). The only place where frequency is specifically invoked is in the use of target covariance values and FR angles appropriate to P-band to generate Table II and Figs. 1 and 2, but this is unlikely to significantly affect our findings. However, the P-band frequency is important in what follows since we express the tradeoff between crosstalk and the channel imbalance term in terms of relative error in AGB using the power law relations described in Section III-D and parameters inferred from P-band data in [6].

TABLE III
SIMULATION PARAMETERS

Description	Symbol	Value		
Standardised Gaussian variable	z_α	1.65	2.33	3.00
Confidence limit of σ^0_{hv} error	-	95%	99%	99.865%
Forest type	-	boreal		tropical
Power law exponent	p	2.2		1.9
Mean value of Faraday rotation	$\overline{\Omega}$	$\pi/3$		0
Maximum and minimum relative error in σ^0_{hv} for 20% AGB error	f_{max}	0.0864		0.1007
	f_{min}	-0.0965		-0.1108
Maximum and minimum relative error in σ^0_{hv} for 10% AGB error	f_{max}	0.0443		0.0514
	f_{min}	-0.0468		-0.0539
NESZ (dB)	-	-27		

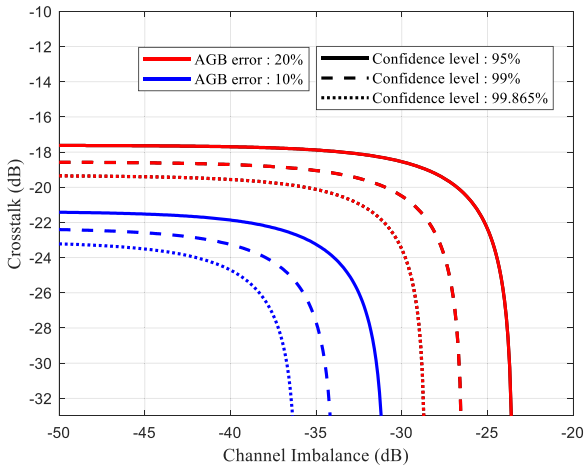

Fig. 3. Tradeoff curves of crosstalk and channel imbalance for three different confidence levels that the AGB is overestimated by less than 20% and 10% for a boreal biomass of 200 t/ha, power law index $p = 2.2$, and mean FR $= \pi/3$.

The following calculations use the simulation parameters summarized in Table III. Fig. 3 shows the crosstalk and channel imbalance tradeoff curves for 95%, 99%, and 99.865% confidence levels that an estimate of AGB does not exceed 20% and 10% of its true value for an AGB of 200 t/ha and power law exponent $p = 2.2$ (boreal), while Fig. 4 shows the corresponding tradeoff curves for underestimation. It is clear that values of crosstalk and channel imbalance that bound overestimation within desired limits guarantee the same for underestimation, as already noted in Section III-D, i.e., controlling overestimation places more stringent requirements on the system errors.

For overestimation, there is only one solution of (19) for a given level of channel imbalance because $b(V_\delta,\ V_\varepsilon) + z_\alpha\sigma_e(V_\delta,\ V_\varepsilon)$ always increases with V_δ. However, for underestimation, there can be two solutions for higher levels of channel

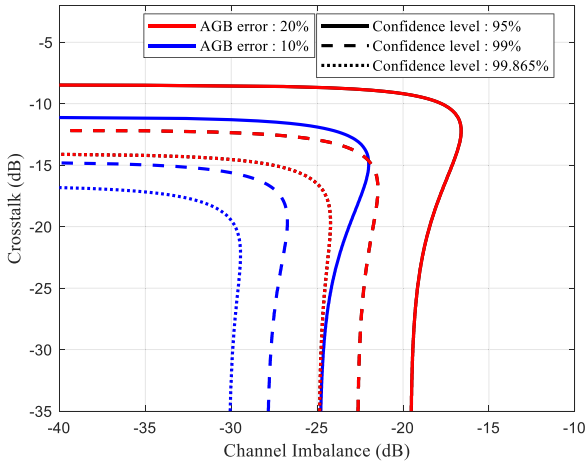

Fig. 4. Tradeoff curves of crosstalk and channel imbalance for three different confidence levels that the AGB is underestimated by less than 20% and 10% for a boreal biomass of 200 t/ha, power law index $p = 2.2$, and mean FR $= \pi/3$.

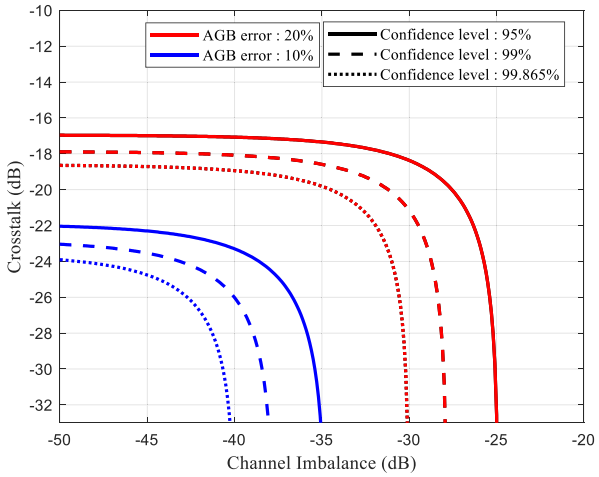

Fig. 5. Tradeoff curves of crosstalk and channel imbalance for three different confidence levels that the AGB is overestimated by less than 20% and 10% for a boreal biomass of 50 t/ha, power law index $p = 2.2$, and mean FR $= \pi/3$.

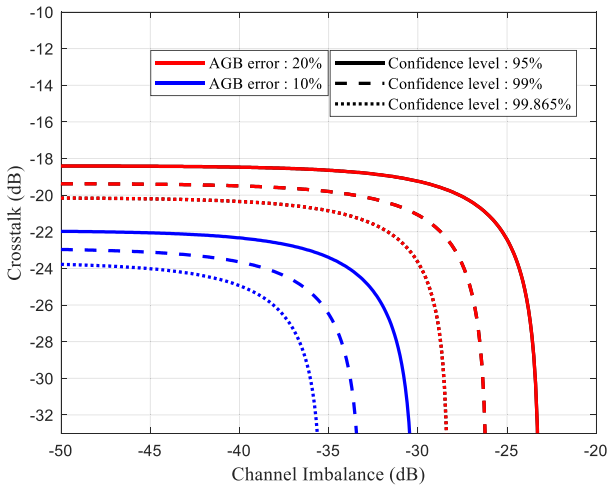

Fig. 6. Tradeoff curves of crosstalk and channel imbalance for three different confidence levels that the AGB is overestimated by less than 20% and 10% for a boreal biomass of 350 t/ha, power law index $p = 2.2$, and mean FR $= \pi/3$.

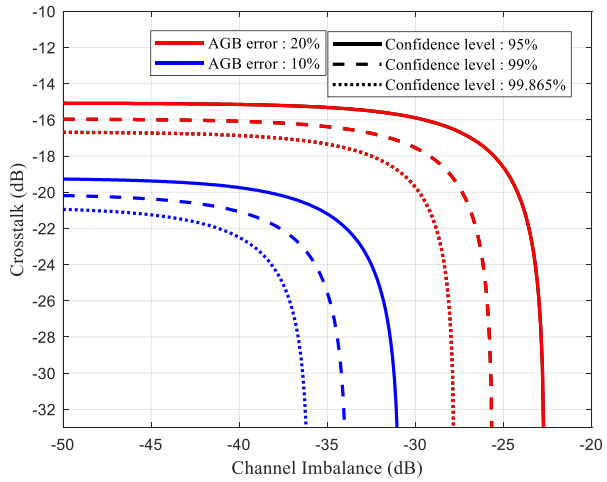

Fig. 7. Tradeoff curves of crosstalk and channel imbalance for three different confidence levels that the AGB is overestimated by less than 20% and 10% for a tropical AGB of 338 t/ha, power law index $p = 1.9$, and mean FR $= 0$.

imbalance because z_α is negative and the bias increases faster than the variance as V_δ increases. As a result, $b(V_\delta, V_\varepsilon) + z_\alpha \sigma_e(V_\delta, V_\varepsilon)$ first increases then decreases as crosstalk increases. This has the counter-intuitive effect that for fixed channel imbalance the underestimation in AGB decreases as crosstalk increases (see Appendix C). This behavior does not contradict the hyperbolic form of (19), but arises from the rotational and logarithmic transformations involved in converting from the standardized form of the hyperbola given in Appendix B back to channel imbalance and crosstalk.

Figs. 5 –8 are similar to Fig. 3 but for the other four values of AGB in Table II. The calculations in Figs. 5 and 6 use a power law exponent $p = 2.2$ (boreal) while Figs. 7 and 8 use $p = 1.9$ (tropical). The corresponding plots for underestimation are not shown since they are similar to Fig. 4, and the conditions keeping the magnitude of overestimation below a given probability always guarantee the same for underestimation.

Several points must be made concerning the figures.

1) The plots shown in Figs. 3–8 can be calculated using a full simulation based on (1) or the analytic approach described above, where the $\sigma^0_{\rm hv}$ errors are taken to be Gaussian with bias and SD given by (11) and (12). In practice, these are indistinguishable. Hence the effects of system errors on errors in $\sigma^0_{\rm hv}$ and AGB can be quickly and accurately quantified and tradeoff curves plotted without the need for complex simulation schemes.
2) As expected, tighter confidence limits on the AGB error require smaller values of the system errors.
3) The maximum permissible size of the channel imbalance terms needs to be significantly smaller than for crosstalk to meet the 10% or 20% constraints on AGB error, as can be seen by the values at which the curves cross the axes.

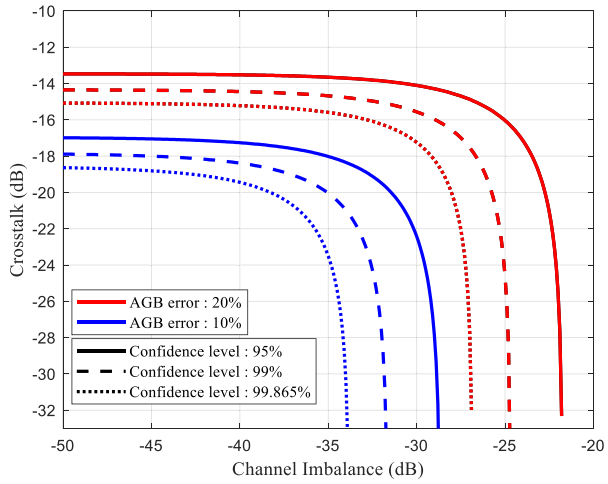

Fig. 8. Tradeoff curves of crosstalk and channel imbalance for three different confidence levels that the AGB is overestimated by less than 20% and 10% for a tropical AGB of 341 t/ha, power law index $p = 1.9$, and mean FR $= 0$.

4) Figs. 3, 5, and 6 indicate that the constraints on channel imbalance are more stringent for lower values of AGB, but the constraints on crosstalk are less so.
5) In principle, the higher value of the power law exponent in boreal forests compared to tropical forests ($p = 2.2$ and 1.9, respectively) means that better system performance is required in boreal forests. In practice, this is weakened because of the dependence of the errors on the terms in the variance-covariance matrix of the target. For example, comparing Fig. 6 (boreal) with Fig. 7 (tropical) shows that similar requirements are found for channel imbalance, but weaker constraints on crosstalk are needed in the tropical case. The differences between Figs. 7 and 8, which are both tropical, are entirely caused by differences in their variance-covariance matrices.
6) In the worst case shown (see Fig. 5), meeting the 99.865% confidence limit that the AGB relative error is less than 20% requires the channel imbalance terms to be smaller than -30.2 dB. The crosstalk requirement is much less demanding: here the worst case (see Fig. 6) requires crosstalk not to exceed -20.16 dB.

VI. Discussion

The BIOMASS mission specifications for crosstalk and channel imbalance terms are currently defined as -30 and -34 dB, respectively, based on the analysis in [4], where they were derived by examining the worst possible case when the system error amplitudes varied over a uniform distribution. Here, however, the errors follow complex Gaussian distributions, in which case their magnitudes obey Rayleigh distributions. A further important difference is that [4] dealt only with the bias in $\sigma_{\rm hv}$ and AGB, and the numerical results did not consider noise, whereas this new analysis treats noise on an equal footing with the system errors and considers both bias and variance. This leads to different conclusions. In [4], the channel imbalance term was found to be the major contributor to bias, whereas here it is noise, while channel imbalance is the dominant contributor to the variance. Hence the quantitative results in [4] cannot be directly compared with those in this article. However, the specifications for the crosstalk and channel imbalance terms derived here are likely to be more realistic, and indicate that the current specifications are unnecessarily demanding. Nonetheless, both analyses make clear that the channel imbalance terms need to be considerably smaller than crosstalk if the BIOMASS mission requirements on AGB accuracy are to be met.

The assumption in this article that the system errors follow complex Gaussian distributions can be questioned, but key aspects of the analysis do not depend on it. The bias in the $\sigma_{\rm hv}$ error (11) does not need it. Moreover, although it played a very useful part in yielding compact expressions for the fourth-order moments involved in the variance calculation (12), the dominant part of the variance comes from the linear term in the ε_i in (3), i.e., $2\sigma_{\rm hv}{\rm Re}(\Sigma_\varepsilon)$. This yields the $2\sigma_{\rm hv}^2 {\rm V}_A$ term in (12a), which is the largest term and does not depend on the Gaussian assumption.

The analysis of $\sigma_{\rm hv}^0$ errors performed in this article is applicable to any SAR frequency, and it is only in the tradeoff curves in Figs. 3–8 that the properties of P-band and the relation between the P-band HV backscattering coefficient and AGB become important. Similar tradeoff curves could have been produced for relative error in $\sigma_{\rm hv}^0$. However, unless the errors in $\sigma_{\rm hv}^0$ can then be related to the accuracy of AGB estimation, they provide little insight into how important such errors are, for example to meeting BIOMASS mission objectives. This motivated the use of a power law to provide this connection, since it has a sound empirical basis [6] and has been used in many earlier studies (an extensive list of such studies using P- and L-band SAR data is provided in the references in [6]). Nonetheless, a reasonable criticism of our results is that they do not reflect current developments in estimation of AGB from polarimetric SAR data, in particular: the combined use of the co-polarised and cross-polarised backscattering coefficient [10], [11]; and the exploitation of ground-cancelled data [9], [12], [13].

The prototype AGB estimation algorithm for BIOMASS [13] combines both of these elements. It assumes separate power law relations between the backscattering coefficient and AGB for each of the HH, HV, and HV channels after the ground and double-bounce returns have been strongly suppressed using coherent subtraction of interferometric signals [12], thus leaving only the backscatter from the forest volume. The parameters controlling the power laws are then estimated by numerical minimization of a cost function.

Analysis of the effects of system errors on this full AGB estimation scheme has not yet been attempted, but some progress has been made towards doing so. For example, empirical analysis based on airborne data indicates that the HV ground-cancelled data still display a power law relationship with AGB, and that, just as was found above, the mean AGB relative error is primarily controlled by noise while its variance is strongly affected by the correlation and phase difference between the channel imbalance terms. There is no obvious difficulty in extending our theoretical analysis to this case, as long as the system errors are stable between the times of the two interferometric acquisitions. The only

proviso is that, since ground-cancellation involves subtracting complex images gathered at different times, it will be necessary to account for differences in FR between the two images.

As regards the combination of co- and cross-polarized channels, in all three cases, $pq = \mathrm{HH}, \mathrm{HV}, \mathrm{VV}$, the relative error in the backscattering coefficient, $(\widehat{\sigma^0_{pq}} - \sigma^0_{pq})/\sigma^0_{pq}$, will be dominated by terms that are linear in the system errors (as shown in this article, these will be the channel imbalance terms for HV, but for the co-polarized channels both channel imbalance and crosstalk terms would make significant contributions [4]). Hence it should be fairly straightforward to extend the theoretical analysis of the HV term in this article to the co-polarized terms, though this remains to be carried out. While this would give insight into what controls these relative errors and their possible sizes and variances, the real difficulty would be to evaluate how the system- and noise-induced errors in each channel interact in the full AGB estimation algorithm. This is likely to be difficult, not least because it is not clear how to perform realistic simulation of the overall algorithm.

Seen against this background, our estimates of the required system performance, as captured by Figs. 3–8, are likely to be conservative, and if the BIOMASS system is compatible with them it will comfortably achieve mission requirements. Current work is extending the analysis to ground-cancelled data, while retaining the use of the HV channel to estimate AGB, and this will make a valuable further step to refining the constraints on the system errors. However, full analysis of the AGB estimation algorithm described in [13] remains a challenging problem.

VII. Conclusion

The cross-polarized backscattering coefficient σ^0_{hv} plays an important role in estimating AGB from SAR data, since numerous studies indicate that the dependence of AGB on σ^0_{hv} can be approximated by a power law relationship (see [6] and references therein). However, system effects (crosstalk, channel imbalance, and system noise) and FR can cause errors in measurements of σ^0_{hv} by a spaceborne SAR system. This article quantifies the mean and variance of these errors for a distributed target characterized by a given covariance matrix when the unknown values of crosstalk, the channel imbalance terms, system noise, and FR obey a joint Gaussian distribution. For system errors whose order of magnitude is likely to be representative of the BIOMASS instrument, first-order expressions for the mean and variance of the σ^0_{hv} errors are shown to be very accurate when compared with simulations that use the full system model. Using these expressions, it is demonstrated that, for the levels of system error expected for BIOMASS, noise is the dominant term causing bias in σ^0_{hv}, while its variance is primarily controlled by channel imbalance.

In addition to confirming the accuracy of the first-order approximations, the simulations indicate that the σ^0_{hv} error distribution is close to Gaussian. Since a Gaussian distribution is completely characterized by its mean and variance, this allows the exceedance probabilities of the σ^0_{hv} error to be quickly and easily calculated using the first-order approximations to these quantities. It is then straightforward to calculate tradeoff curves showing how crosstalk and channel imbalance need to be related to keep the relative error in σ^0_{hv} below a given value at a given level of significance.

Based on a power law relation between AGB and σ^0_{hv}, associated tradeoff curves can be calculated that show the acceptable joint levels of channel imbalance and crosstalk that ensure the relative error in AGB is less than a given percentage for a given level of significance. These are provided for 20% and 10% relative error for a range of AGB and for conditions corresponding to both boreal and tropical forests, in which different power law exponents are needed.

It must be stressed that the quantitative tradeoff calculations offer only an approximate and conservative guide to the required constraints on the size of the BIOMASS system errors, for two main reasons.

1) Significantly better estimation of AGB from the σ^0_{hv} signal is achieved after removing contamination by the ground using coherent subtraction of signals from different times [12]. This requires a modified analysis because FR is likely to differ between the two times.
2) The most recent prototype algorithm [13] for estimating AGB from BIOMASS data uses ground-cancelled data and combines information from all three of the HH, HV, and VV channels, each of which is assumed to be related to AGB by an independent power law. Assessing the effects of system errors on this AGB estimation scheme provides a much greater challenge.

Appendix A
First-Order Estimates of the Mean and Variance of the Error in $\sigma_{\mathbf{hv}}$

From (5), the error in σ_{hv} can be written as

$$\begin{aligned} e = {} & \sigma_{\mathrm{hv}} \left(2\mathrm{Re}\,(A) + |\mathrm{A}|^2\right) + P|B|^2 \\ & + 2\mathrm{Re}\left\{B^* \left[X\left(\sigma_{\mathrm{hh}} + Re^{j\theta}\right) + Y\left(\sigma_{\mathrm{vv}} + \mathrm{Re}^{-j\theta}\right)\right]\right\} \\ & + \sigma_{\mathrm{hh}}|X|^2 + \sigma_{\mathrm{vv}}|Y|^2 + 2\mathrm{Re}\left\{\mathrm{Re}^{j\theta} XY^*\right\} + \sigma_n/2 \end{aligned} \quad \text{(A1)}$$

where $P = \sigma_{\mathrm{hh}} + \sigma_{\mathrm{vv}} + 2R\cos\theta$. Since $A, B, X,$ and Y are zero-mean, and the A and B terms are uncorrelated with X and Y, the expectation of e is

$$\langle e\rangle = \sigma_{\mathrm{hv}}\, V_A + PV_B + \sigma_{\mathrm{hh}} V_X + \sigma_{\mathrm{vv}} V_Y + 2R\cos\theta C_{XY} + \frac{\sigma_n}{2}. \quad \text{(A2)}$$

From (A1) and (A2)

$$\begin{aligned} e - \langle e\rangle = {} & \sigma_{\mathrm{hv}} \left(2\mathrm{Re}\,(A) + |A|^2 - V_A\right) + P\left(|B|^2 - V_B\right) \\ & + \sigma_{\mathrm{hh}}\left(|X|^2 - V_X\right) + \sigma_{vv}\left(|Y|^2 - V_Y\right) \\ & + 2\mathrm{Re}\left\{\mathrm{Re}^{j\theta} XY^*\right\} \\ & - 2R\cos\theta\, C_{XY} \\ & + 2\mathrm{Re}\left\{B^*\left[X\left(\sigma_{\mathrm{hh}} + \mathrm{Re}^{j\theta}\right) + Y\left(\sigma_{\mathrm{vv}} + \mathrm{Re}^{-j\theta}\right)\right]\right\}. \end{aligned} \quad \text{(A3)}$$

The variance of e can be split into terms coming solely from channel imbalance, solely from crosstalk and interaction between the two. The first is given by

$$\begin{aligned} V_{e1} &= \langle \sigma_{\rm hv}^2 \Big(A + A^* + |A|^2 - V_A \Big)^2 + P^2 \Big(|B|^2 - V_B \Big)^2 \rangle \\ &\quad + \langle 2P\sigma_{\rm hv} \Big(A + A^* + |A|^2 - V_A \Big) \Big(|B|^2 - V_B \Big) \rangle \\ &= \sigma_{\rm hv}^2 \left(V_A^2 + 2V_A \right) + P^2 V_B^2 + 2\sigma_{\rm hv} P |C_{AB}|^2. \end{aligned} \tag{A4}$$

The second is given by

$$\begin{aligned} V_{e2} &= \left\{ \sigma_{\rm hh} \left(XX^* - V_X \right) + \sigma_{\rm vv} \left(YY^* - V_X \right) \right. \\ &\quad \left. + R \left(XY^* e^{j\theta} + X^* Y e^{-j\theta} - 2\cos\theta C_{XY} \right) \right\}^2 \\ &= \sigma_{hh}^2 \, V_X^2 + \sigma_{vv}^2 V_Y^2 + 2R^2 \left\{ V_X V_Y + C_{XY}^2 \cos 2\theta \right\} \\ &\quad + 2\sigma_{\rm hh}\sigma_{\rm vv} C_{XY}^2 + 4R\cos\theta C_{XY} \left(\sigma_{\rm hh} V_X + \sigma_{\rm vv} V_Y \right). \end{aligned} \tag{A5}$$

All the interaction terms in the square of (A3) have expectation 0 except for the square of the last term

$$\begin{aligned} &\left\langle \left\{ B^* \left[X \left(\sigma_{\rm hh} + {\rm Re}^{j\theta} \right) + Y \left(\sigma_{\rm vv} + {\rm Re}^{-j\theta} \right) \right] \right. \\ &\left. + B \left[X^* \left(\sigma_{\rm hh} + {\rm Re}^{-j\theta} \right) + Y^* \left(\sigma_{\rm vv} + {\rm Re}^{j\theta} \right) \right] \right\}^2 \rangle. \end{aligned}$$

Here, the only part not averaging to 0 is from the product of the 2 terms involving square brackets, whose expectation is

$$\begin{aligned} V_{e3} &= 2V_B \{ V_X \left(\sigma_{\rm hh} + Re^{j\theta} \right) \left(\sigma_{\rm hh} + {\rm Re}^{-j\theta} \right) \\ &\quad + V_Y \left(\sigma_{\rm vv} + {\rm Re}^{-j\theta} \right) \left(\sigma_{\rm vv} + {\rm Re}^{j\theta} \right) \\ &\quad + C_{XY} [\left(\sigma_{\rm hh} + {\rm Re}^{j\theta} \right) \left(\sigma_{\rm vv} + {\rm Re}^{j\theta} \right) \\ &\quad + \left(\sigma_{\rm vv} + {\rm Re}^{-j\theta} \right) \left(\sigma_{\rm hh} + {\rm Re}^{-j\theta} \right)] \} \\ &= 2V_B \{ V_X \sigma_{\rm hh}^2 + V_Y \sigma_{\rm vv}^2 + 2C_{XY} \sigma_{\rm hh} \sigma_{\rm vv} \\ &\quad + 2R\cos\theta \left(V_X \sigma_{\rm hh} + V_Y \sigma_{\rm vv} + C_{XY} \left(\sigma_{\rm hh} + \sigma_{\rm vv} \right) \right) \\ &\quad + R^2 \left(V_X + V_Y + 2C_{XY} \cos 2\theta \right) \}. \end{aligned} \tag{A6}$$

The overall variance of the error is then given by (A4) + (A5) + (A6).

Appendix B
Hyperbolic Form of the Tradeoff Curves

Equation (19) quantifies the tradeoff between V_ε and V_δ that keeps the error in $\sigma_{\rm hv}$ below $f\sigma_{\rm hv}$ with probability α

$$z_\alpha \sigma_e \left(V_\delta, \, V_\varepsilon \right) + b \left(V_\delta, \, V_\varepsilon \right) = f\sigma_{\rm hv}. \tag{B1}$$

Under the first-order approximations (11) and (12)

$$b = a_1 V_\varepsilon + a_2 V_\delta + \sigma_n/2 \tag{B2a}$$

$$\sigma_e^2 = b_1 V_\varepsilon + b_2 V_\varepsilon^2 + b_3 V_\delta^2 + b_4 V_\varepsilon V_\delta. \tag{B2b}$$

Hence

$$\sigma_e^2 = \left(\frac{f\sigma_{\rm hv}}{z_\alpha} - \frac{b}{z_\alpha} \right)^2 = \left(A_0 - A_1 V_\varepsilon - A_2 V_\delta \right)^2 \tag{B3}$$

where

$$\begin{aligned} A_0 &= \frac{f\sigma_{\rm hv} - \sigma_n/2}{z_\alpha} \\ A_1 &= \frac{a_1}{z_\alpha} \\ A_2 &= \frac{a_2}{z_\alpha}. \end{aligned}$$

(B3) can then be rewritten as

$$\begin{aligned} &\left(b_2 - A_1^2 \right) V_\varepsilon^2 + \left(b_3 - A_2^2 \right) V_\delta^2 \\ &+ \left(b_4 - 2A_1 A_2 \right) V_\varepsilon V_\delta + \left(b_1 + 2A_0 A_1 \right) V_\varepsilon \\ &+ 2A_0 A_2 V_\delta - A_0^2 = 0. \end{aligned}$$

Write this as

$$P_1 V_\varepsilon^2 + P_2 V_\delta^2 + P_3 V_\varepsilon V_\delta + P_4 V_\varepsilon + P_5 V_\delta - P_6 = 0. \tag{B4}$$

Rotating the axes using the transform

$$\begin{pmatrix} V_\varepsilon \\ V_\delta \end{pmatrix} = \begin{pmatrix} \cos\varphi & \sin\varphi \\ -\sin\varphi & \cos\varphi \end{pmatrix} \begin{pmatrix} X \\ Y \end{pmatrix} \tag{B5}$$

where $\tan 2\varphi = \frac{P_3}{P_2 - P_1}$, converts this to the form

$$C_1 X^2 + C_2 Y^2 + C_3 X + C_4 Y - C_0 = 0 \tag{B6}$$

where

$$\begin{aligned} C_1 &= P_1 c^2 + P_2 s^2 - P_3 cs \\ C_2 &= P_1 s^2 + P_2 c^2 + P_3 cs \\ C_3 &= P_4 c - P_5 s \\ C_4 &= P_4 s + P_5 c \\ C_0 &= P_6 \end{aligned}$$

with $c = \cos\varphi$ and $s = \sin\varphi$.

This can be converted into the standard form of a conic by completing squares and normalizing

$$\frac{\left(X + \frac{C_3}{2C_1} \right)^2}{B_1} + \frac{\left(Y + \frac{C_4}{2C_2} \right)^2}{B_2} = 1 \tag{B7}$$

where $B_1 = \frac{C_0 + \frac{C_3^2}{4C_1} + \frac{C_4^2}{4C_2}}{C_1}$ and $B_2 = \frac{C_0 + \frac{C_3^2}{4C_1} + \frac{C_4^2}{4C_2}}{C_2}$.

Because B_1 is positive and B_2 is negative, this is a hyperbola. (B7) can then be expressed in terms of V_ε and V_δ by inverting (B5) and substituting for X and Y. Since we are characterizing the size of the crosstalk errors as $p_\delta = 3\sigma = 3\sqrt{V_\delta/2}$, where σ is the SD of the real and imaginary parts of the error, we finally need to replace V_δ by $p_\delta^2/4.5$, and similarly for V_ε.

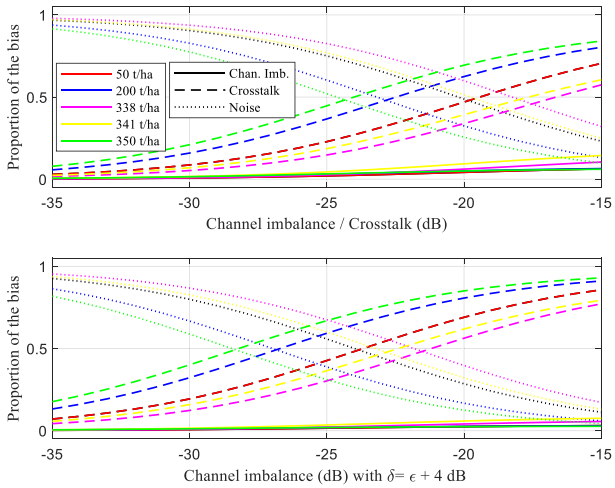

Fig. 9. Proportion of the mean error in $\sigma^0_{\rm hv}$ given by the V_δ, V_ε, and noise terms in (11) against the channel imbalance term, with crosstalk fixed to be equal to the channel imbalance term (top) and 4 dB higher than the channel imbalance term (bottom) for a range of values of AGB and for NESZ $= -27$ dB.

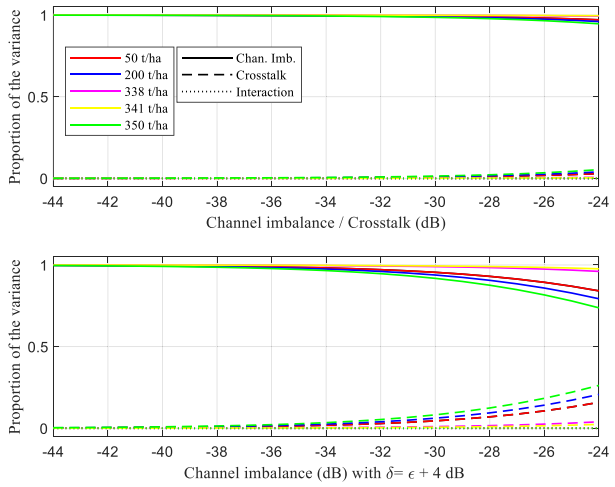

Fig. 10. Proportion of the variance of the error in $\sigma^0_{\rm hv}$ given by the V_δ , V_ε, and interaction terms in (12) against the channel imbalance term, with crosstalk fixed to be equal to the channel imbalance term (top) and 4 dB higher than the channel imbalance term (bottom), for a range of values of AGB and for NESZ $= -27$ dB.

Appendix C
Proportions of the Bias and Variance of the $\sigma_{\rm hv}$ Error Contributed by Channel Imbalance, Crosstalk, and Noise

Fig. 9 shows the proportion of the mean error in σ_{hv} coming from the V_δ, V_ε and noise terms in (11) when the channel imbalance and crosstalk terms are equal (top) and when the crosstalk is 4 dB higher than the channel imbalance terms (bottom) for a range of AGB values. Noise always dominates the mean error unless crosstalk exceeds -25 dB (upper case) and -28.5 dB (lower case), respectively. The channel imbalance contribution is always small. Fig. 10 indicates that the channel imbalance (12a) always dominates the variance and the interaction term (12c) is negligible.

Acknowledgment

The authors would like to thank L. Villard of CESBIO for preparing and providing the AfriSAR and TropiSAR data used in this article and ESA for supporting these airborne campaigns.

References

[1] S. Quegan *et al.*, "Report for mission selection: BIOMASS," Eur. Space Agency, Noordwijk, The Netherlands, 2012.
[2] S. Quegan *et al.*, "The European space agency BIOMASS mission: Measuring forest above-ground biomass from space," *Remote Sens. Environ.*, vol. 227, pp. 44–60, 2019.
[3] A. Freeman, "Calibration of linearly polarized polarimetric SAR data subject to faraday rotation," *IEEE Trans. Geosci. Remote Sens.*, vol. 42, no. 8, pp. 1617–1624, Aug. 2004. doi: 10.1109/TGRS.2004.830161.
[4] S. Quegan and M. R. Lomas, "The interaction between faraday rotation and system effects in synthetic aperture radar measurements of backscatter and biomass," *IEEE Trans. Geosci. Remote Sens.*, vol. 53, no. 8, pp. 4299–4312, Aug. 2015. doi: 10.1109/TGRS.2015.2395138.
[5] P. López-Dekker *et al.*, "BIOMASS end-to-end mission performance simulator." in *Proc. IEEE Int. Geosci. Remote Sens. Symp.*, 2011, pp. 4249–4252.
[6] M. Schlund, K. Scipal, and S. Quegan, "Assessment of a power law relationship between P-band SAR backscatter and aboveground biomass and its implications for BIOMASS mission performance," *IEEE J. Sel. Top. Appl. Earth Obs. Remote Sens.*, vol. 11, no. 10, pp. 3538–3547, Oct. 2018, doi: 10.1109/JSTARS.2018.2866868.
[7] P. C. Dubois-Fernandez *et al.*, "The TropiSAR airborne campaign in french guiana: Objectives, description, and observed temporal behavior of the backscatter signal," *IEEE Trans. Geosci. Remote Sens.*, vol. 50, no. 8, pp. 3228–3241, Aug. 2012, doi: 10.1109/TGRS.2011.2180728.
[8] N. Labrière *et al.*, "In situ reference datasets from the TropiSAR and AfriSAR campaigns in support of upcoming spaceborne biomass missions," *IEEE J. Sel. Top. Appl. Earth Obs. Remote Sens.*, vol. 11, no. 10, pp. 3617–3627, Oct. 2018, doi: 10.1109/JSTARS.2018.2851606.
[9] F. Banda *et al.*, "The BIOMASS level 2 prototype processor: Design and experimental results of above-ground biomass estimation," *Remote Sens.*, vol. 12, no. 6:985, Mar. 2020.
[10] M. Truong-Loï, S. Saatchi, and S. Jaruwatanadilok, "Soil moisture estimation under tropical forests using UHF radar polarimetry," *IEEE Trans. Geosci. Remote Sens.*, vol. 53, no. 4, pp. 1718–1727, Apr. 2015, doi: 10.1109/TGRS.2014.2346656.
[11] NASA-ISRO SAR (NISAR) Mission Science Users' Handbook, Jet Propulsion Lab., California Inst. Technol., Pasadena, CA, USA, 2018.
[12] M. Mariotti d'Alessandro, S. Tebaldini, S. Quegan, M. J. Soja, L. M. H. Ulander, and K. Scipal, "Interferometric ground cancellation for above ground biomass estimation," *IEEE Trans. Geosci. Remote Sens.*, vol. 58, no. 9, pp. 6410–6419, Sep. 2020, doi:10.1109/TGRS.2020.2976854.
[13] M. J. Soja *et al.*. "Mapping above-ground biomass in tropical forests with ground-cancelled P-band SAR and limited reference data," *Remote Sens. Environ.*, vol. 253, 2020, Art. no. 112153.

Zhirong Men (Member, IEEE) received the Ph.D. degree in information and communication engineering from Beihang University, Beijing, China, in 2018.

From 2018 to 2020, he was a Postdoctoral Researcher with the School of Electronics and Information Engineering, Beihang University, where he has been a Lecturer since October 2020. From 2019 to 2020, he was a Visiting Researcher with the School of Mathematics and Statistics, University of Sheffield, Sheffield, U.K., working with Prof. Shaun Quegan on BIOMASS. His current research interests include novel spaceborne synthetic aperture radar high-resolution spaceborne SAR formation, and SAR data application.

Shaun Quegan received the B.A. and M.Sc. degrees in mathematics from the University of Warwick, Coventry, U.K., in 1970 and 1972, respectively, and the Ph.D. degree in ionospheric physics from the University of Sheffield, Sheffield, U.K., in 1982.

From 1982 to 1986, he was a Research Scientist with the Marconi Research Centre, Great Baddow, U.K., and led the Remote Sensing Applications Group, from 1984 to 1986. He established the SAR Research Group with the University of Sheffield in 1986, and was awarded a Professorship in 1993. In 2001, he became the Director of the U.K. National Environmental Research Council Centre for Terrestrial Carbon Dynamics, which was merged into the U.K. National Centre for Earth Observation in 2008, in which he led the Carbon Cycle Theme. He is a Proposer of the European Space Agency BIOMASS mission, launching in 2023, and chairs the Mission Advisory Group. His research interests include exploiting many sorts of EO technology to give greater quantitative understanding of the carbon cycle, especially the role of forests, and he has served on numerous national and international committees advising on climate and Earth Observation by satellites.

Guido Riembauer received the Bachelor's degree in geography from the University of Göttingen, Göttingen, Germany, in 2012 and the Master's degree in geoinformation and visualisation from the University of Potsdam, Potsdam, Germany, in 2015. He specialised in radar remote sensing and earth observation analysis with open source software.

From 2018 to 2020, he contributed to the scientific preparation of the BIOMASS mission during his traineeship at the Earth Observation Directorate of the European Space Agency. In 2020, he joined Mundialis in Bonn, Germany.

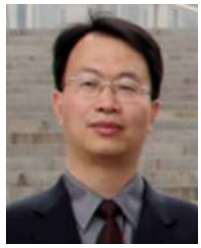

Jie Chen (Senior Member, IEEE) received the B.S. and Ph.D. degrees in information and communication engineering from Beihang University, Beijing, China, in 1996 and 2002, respectively.

From 2004, he was an Associate Professor with the School of Electronics and Information Engineering, Beihang University. He was a Visiting Researcher with the School of Mathematics and Statistics, University of Sheffield, Sheffield, U.K., from 2009 to 2010, working on ionospheric effects on low-frequency space radars that measure forest biomass and ionospheric electron densities. Since July 2011, he has been a Professor with the School of Electronics and Information Engineering, Beihang University. His current research interests include multimodal remote sensing data fusion; topside ionosphere exploration with spaceborne HF/VHF-SAR system; high-resolution spaceborne SAR image formation, and SAR image quality enhancement.